NeuroImage 105 (2015) 257–268

Contents lists available at ScienceDirect

NeuroImage

journal homepage: www.elsevier.com/locate/ynimg

Improved image registration by sparse patch-based deformation estimation

Minjeong Kim [a], Guorong Wu [a], Qian Wang [b], Seong-Whan Lee [c], Dinggang Shen [a,c,*]

[a] Department of Radiology and BRIC, University of North Carolina at Chapel Hill, NC 27599, USA
[b] Med-X Research Institute, School of Biomedical Engineering, Shanghai Jiao Tong University, Shanghai 200030, China
[c] Department of Brain and Cognitive Engineering, Korea University, Seoul, Republic of Korea

ARTICLE INFO

Article history:
Accepted 8 October 2014
Available online 16 October 2014

Keywords:
Deformable image registration
Sparse representation
Initial deformation prediction

ABSTRACT

Despite intensive efforts for decades, deformable image registration is still a challenging problem due to the potential large anatomical differences across individual images, which limits the registration performance. Fortunately, this issue could be alleviated if a good initial deformation can be provided for the two images under registration, which are often termed as the moving subject and the fixed template, respectively. In this work, we present a novel patch-based initial deformation prediction framework for improving the performance of existing registration algorithms. Our main idea is to estimate the initial deformation between subject and template in a patch-wise fashion by using the sparse representation technique. We argue that two image patches should follow the same deformation toward the template image if their patch-wise appearance patterns are similar. To this end, our framework consists of two stages, i.e., the training stage and the application stage. In the training stage, we register all training images to the pre-selected template, such that the deformation of each training image with respect to the template is known. In the application stage, we apply the following four steps to efficiently calculate the initial deformation field for the new test subject: (1) We pick a small number of key points in the distinctive regions of the test subject; (2) for each key point, we extract a local patch and form a coupled appearance-deformation dictionary from training images where each dictionary atom consists of the image intensity patch as well as their respective local deformations; (3) a small set of training image patches in the coupled dictionary are selected to represent the image patch of each subject key point by sparse representation. Then, we can predict the initial deformation for each subject key point by propagating the pre-estimated deformations on the selected training patches with the same sparse representation coefficients; and (4) we employ thin-plate splines (TPS) to interpolate a dense initial deformation field by considering all key points as the control points. Thus, the conventional image registration problem becomes much easier in the sense that we only need to compute the remaining small deformation for completing the registration of the subject to the template. Experimental results on both simulated and real data show that the registration performance can be significantly improved after integrating our patch-based deformation prediction framework into the existing registration algorithms.

Introduction

Deformable image registration has been widely used in many neuroscience and clinical studies, such as quantitative measurement of inter-group structural difference and the identification of abnormalities in disease-affected brains. Specifically, by using deformable registration methods, extrinsic anatomical variations among a population of subjects can be minimized, while the remaining intrinsic structure differences are regarded as imaging-based biomarkers to quantitatively measure the anatomical differences between clinic groups. Since the deformation field characterizes the local structure changes toward the reference space, many imaging-based approaches extract the morphometric patterns from deformation fields for group comparison or disease diagnosis (Freeborough and Fox, 1998; Downhill et al., 2000; Thompson et al., 2001; Frisoni et al., 2002; Job et al., 2003; Merschhemke et al., 2003; Verma et al., 2005; Shen et al., 2004; Chen et al., 2009; Qiao et al., 2009).

Although numerous registration methods have been proposed in the last decades, it is still challenging to register two individual images with large anatomical differences. In general, most deformable registration methods, regardless of intensity-based (Thirion, 1998; Rueckert et al., 1999; Johnson and Christensen, 2002) or feature-based methods (Rohr, 1999; Shen and Davatzikos, 2002, 2003; Shen, 2004; Ou et al.,

* Corresponding author.
E-mail addresses: mjkim@med.unc.edu (M. Kim), grwu@med.unc.edu (G. Wu), wang.qian@sjtu.edu.cn (Q. Wang), swlee@image.korea.ac.kr (S.-W. Lee), dgshen@med.unc.edu (D. Shen).

http://dx.doi.org/10.1016/j.neuroimage.2014.10.019
1053-8119/

2011), aim to optimize the deformation field by minimizing the intensity and structural differences between template and deformed subject images. As the image registration is a complex ill-posed problem, many regularization constraints upon the deformation field have also been proposed to cast image registration to the well-posed scenario, e.g., elastic energy (Bajcsy and Kovacic, 1989; Davatzikos, 1997), viscous fluid (Christensen et al., 1994, 1996), biomechanical model (Ferrant et al., 2000), Laplacian term (Shen and Davatzikos, 2002, 2003), or even statistical prior (Loeckx et al., 2003; Rueckert et al., 2003; Xue et al., 2006; Albrecht et al., 2008; Glocker et al., 2009). However, the optimization of the deformation field from scratch, as in many conventional methods, is often very complicated and challenging to solve, especially the deformation pathway between two images is large. Therefore, conventional image registration encounters the following issues: (1) long computation time needed for estimating possible large deformations, and (2) high vulnerability of being trapped in local minima. Recently, symmetric image registration methods (Avants et al., 2008; Wu et al., 2014) were proposed to partially alleviate these challenges by estimating a deformation pathway from both ends of the two images (i.e., subject and template) simultaneously, such that the two images can be deformed to meet at the middle point of their deformation pathways. However, the estimation of the half-way deformation for each image still suffers from the very large anatomical differences.

Good initialization of deformation field is effective to tackle the above-mentioned issues, especially when two images have large appearance discrepancies. To this end, learning-based methods have been proposed in the past years to help detect corresponding landmarks or predict an initial shape of the object. For example, an automatic landmark detection method (Neu and Toga, 2008) was proposed to learn the statistical relation between the local appearance and landmarks to guide the identification of the landmarks in the new subjects. The other method, called shape regression machine (Zhou and Comaniciu, 2007), was designed to provide the good initialization of the target object detection by the nonlinear regressors learned upon the correlation between image appearance and their respective shapes. However, the complexity of such applications regarding the initialization of either landmarks or shapes is relatively low, compared to the prediction of dense deformation field in our application.

In the last decade, several deformation prediction methods have been developed for providing the initial deformation prior to deformable brain image registration. Thus the registration method only needs to estimate a small segment of deformation. Since the estimated initial deformation makes the template image and the deformed subject image very close to each other, the remaining (small) deformation can be effectively estimated by many of the existing registration algorithms. Specifically, several learning-based registration methods for predicting the initial deformation field have been proposed by investigating the correlation between image appearances and deformation statistics (Tang et al., 2009; Kim et al., 2012). Although promising improvements on registration results have been achieved, these learning-based methods intended to capture the very high-dimensional image appearances and deformation fields by only using simple statistical models, such as principal component analysis (PCA). Thus, these learned-based models have limitations in prediction accuracy. For example, RABBIT (Tang et al., 2009) computed image similarity based on the entire images to automatically determine the most similar intermediate template with respect to a certain subject. Then, the registration of the subject with the template was reduced to a simple problem of registering the subject to the estimated intermediate template, since the registration between the intermediate template and the template has been pre-computed already. On the other hand, more advanced method (Kim et al., 2012) has been proposed to learn the relationship between image appearances and deformation fields from the training images by support vector regression (SVR) model (Smola and Scholköpf, 2004). Specifically, given a new subject image, the learned SVR model will automatically predict the initial deformation field based on the appearance of this subject image. Then, the estimated initial deformation field can be used to warp the template for generating a subject-specific intermediate template. In this way, the subject image only needs to be registered with this intermediate template, thus significantly reducing the complexity of original registration problem. However, in this method, the regression model was used to learn the relationship between the whole image appearance and the entire deformation field, which is limited to completely capture the complex local deformation characteristics in the training stage. Moreover, most previous learning-based methods often lack the ability of incremental learning, thus the training dataset has to be fixed and the inclusion of new training samples requires re-training of the model.

Recently, sparse patch-based approaches have been widely applied to image analysis studies, including multi-atlas segmentation, inpainting, denoising, and super-resolution problems (Zongben and Jian, 2010; Coupé et al., 2011; Rousseau et al., 2011; Chatterjee and Milanfar, 2012; Zhang et al., 2012). Given a sufficient number of patches from the training images, each patch in the subject image can be well-represented by a sparse linear combination of similar patches from the training images. If two image patches are similar in appearances, they could be coming from the same anatomical structures of different images and thus can be regarded as correspondences to each other. The success of these sparse patch-based approaches motivates us to apply this technique to correlate image appearances with deformations at the scale of local patch, in order to provide more accurate initial deformation field for image registration.

In this paper, we propose a novel patch-based deformation prediction framework to provide a good initial deformation field between template and subject images for augmenting the performance of registering two images. That is, our method is able to provide a good deformation field for initializing the image registration, which can be further refined by many of the existing registration methods. Specifically, we argue that (1) if a patch in the subject image is similar (in appearances) to a certain patch in a training image, the corresponding points for these two patches toward the same template should be highly related; and (2) given a sufficient number of training images, each patch in the subject image can identify several similar instances from the properly selected training images via the sparse learning technique.

Specifically, there are two stages in our proposed framework, i.e., the training stage and the application stage. In the training stage, a large number of training images are carefully registered to a selected template. Thus, we obtain the dense deformation field for each training image. In the application stage, for registering a new subject image with the same selected template, we first select a small number of key points at the distinctive regions of this subject image. Then, for each key point in the subject image, we extract the image patch, centered at the underlying key point. Then, we adaptively construct the coupled dictionary for the underlying point where each atom in the dictionary consists of image intensity patches and the respective deformations obtained from training images. Next, the subject image patch can be sparsely represented by a linear combination of training image patches in the dictionary, where we apply the same sparse coefficients to the respective deformations in the dictionary to predict the deformation for the subject image patch. After we repeat the same procedure for each subject key point, we use thin-plate splines (TPS) (Bookstein, 1989) to interpolate a dense deformation field, which is used as the initialization to allow the registration algorithm estimating the remaining small segment of deformations toward the template image. Experimental results on both simulated and real data show that our patch-based deformation prediction framework can improve the registration accuracy for several mainstream registration methods, including HAMMER (Shen and Davatzikos, 2002, 2003), diffeomorphic Demons (Vercauteren et al., 2009), FNIRT (Andersson et al., 2008), ART (Ardekani et al., 2005), and SyN (Avants et al., 2008).

This paper is organized as follows. In Methods, we first overview our proposed sparse patch-based deformation estimation framework, followed by the details on the construction of the coupled patch-based appearance-deformation dictionary (Key point selection and coupled dictionary construction) and the prediction of local deformations of subject patches via sparse learning (Extraction of patch on each key point). We show the experimental results on both real and simulated data in Experimental results. Finally, in Discussion and conclusion, we conclude our novel patch-based deformation prediction framework, along with some extensive discussions.

Methods

In this section, we present a general framework to improve the performances of the existing registration algorithm by predicting a good initial deformation field. The overview of our sparse patch-based deformation estimation framework is provided in Overview of sparse patch-based deformation estimation framework. For predicting the initial deformation, we construct the coupled dictionary (consisting of both patch-based image appearances and their respective deformations) in Key point selection and coupled dictionary construction, and then predict the deformation field via sparse learning in Deformation prediction by sparse patch representation. Finally, we summarize our learning-based registration framework in Summary of our learning-based registration framework.

Overview of sparse patch-based deformation estimation framework

The goal of deformable registration is to estimate a dense deformation field f_S for registering the subject image I_S to the template I_T, where $f_S(x)$ denotes the deformation of the point x in the template image domain Ω_T. In our learning-based registration framework, the overall deformation field f_S is decomposed into two parts, i.e., $f_S(x) = f_S^E(x) + f_S^R(x)$, where f_S^E is the predicted initial deformation field and f_S^R is the remaining deformation field. It is worth noting that most existing registration methods start without any initial prediction, i.e., $f_S^E(x) = 0, \forall\, x \in \Omega_T$. Although f_S^E can be predicted by some previous learning-based methods (Tang et al., 2009; Kim et al., 2012), the details of local deformations could be missed due to the use of global models to represent the entire deformation field in those methods.

We hereby propose a novel patch-based approach to adaptively predict the initial deformation f_S^E as illustrated in Fig. 1. Specifically, in the training stage, a number of training images $\{I_m | m = 1, \ldots, N\}$ are first registered with a selected template I_T by the state-of-the-art registration algorithms, such as HAMMER (Shen and Davatzikos, 2002, 2003), diffeomorphic Demons (Vercauteren et al., 2009), FNIRT (Andersson et al., 2008), ART (Ardekani et al., 2005), and SyN (Avants et al., 2008). Note that the training is conducted offline. Hence, it allows us to utilize additional sources of information to achieve more accurate image registration. For example, we can use optimal registration parameters for each pairwise image registration in the training stage. Moreover, we can also manually annotate a number of landmarks in

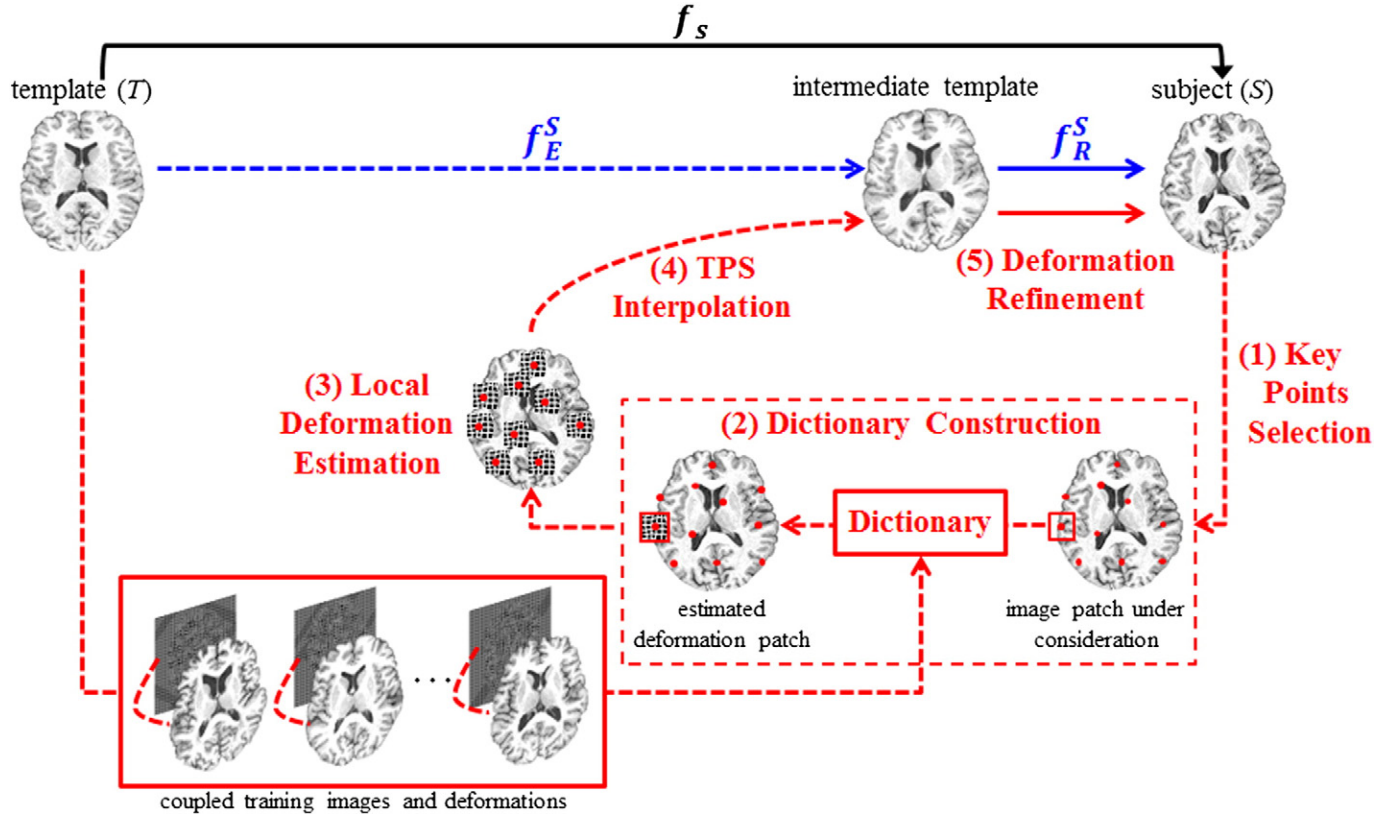

Fig. 1. Illustration of our proposed learning-based registration framework, using the sparse patch-based deformation initialization. In the training stage, we register all training images to the template image, and obtain a set of deformation fields (see the solid red box). In the application stage, to predict the initial deformation field for the new testing subject, we first extract a set of key points in the new testing subject image. Then, for each key point, we adaptively construct a coupled dictionary from the training images, where each coupled atom includes both appearance and deformation of the same image patch (see the red dash box). After calculating the sparse coefficients in representing the appearance of the patch of each subject key point based on the constructed dictionary, we can predict the deformation for this subject key point by applying the same coefficients (estimated from the appearance) to the respective deformations in the coupled dictionary. Then, the dense deformation field can be interpolated via TPS, and further used as the initial deformation field to warp the template to generate the intermediate template. Finally, we can employ a certain existing registration algorithm to estimate the remaining small deformation between the generated intermediate template and the new test subject, thus completing the estimation of the entire deformation pathway.

each training image and use these established correspondences to improve the image registration.

Then, the deformation field f_m from the template I_T to each subject I_m can be acquired, therefore obtaining a set of deformation fields $F = \{f_m | m = 1, \ldots, N\}$. Accordingly, we know the deformation field of each training image with respect to the template (as shown as the red solid box in the left-bottom corner of Fig. 1). Then, for any given subject image, its registration to the template image can be completed by the following five steps:

1) A set of K key points are first selected automatically in the subject image I_S, and denoted as $X = \{x_k | k = 1, \ldots, K\}$. It is worth noting that we refer x_k to the k-th key point in subject I_S in the following text.
2) We adaptively construct a coupled dictionary for each subject key point x_k, where each coupled atom in the dictionary consists of a pair of patch-based image appearance and its associated deformation to the template image.
3) The initial deformation on each key point of a new testing subject can be predicted via the sparse representation technique, as detailed in Deformation prediction by sparse patch representation.
4) Given the estimation of the initial deformations on the key points of the subject image, we apply TPS to interpolate the initial dense deformation field f_S^E for the whole subject image.
5) We deform the template image I_T by following the predicted initial deformation field f_S^E to generate an intermediate template for the subject image. It is worth noting that the shape difference between the generated intermediate template and the subject image can be small, as illustrated by the two brain images in the top-right of Fig. 1, thus making the refinement of registration by the existing registration algorithms much easier.

Many existing registration algorithms can be employed to estimate the remaining deformation f_S^R for completing the refinement of the overall registration. It is worth noting that the use of the generated intermediate template reduces the complexity of the conventional image registration (which often registers the subject image directly to the template image), since only small remaining deformation field needs to be estimated.

Key point selection and coupled dictionary construction

To construct the locally-adaptive coupled dictionary for each subject key point, we first register N training images to the template I_T, for obtaining a set of deformation fields from all training images. It is worth noting that most mainstream registration methods (Shen and Davatzikos, 2002; Ardekani et al., 2005; Andersson et al., 2008; Avants et al., 2008; Vercauteren et al., 2009) can be used for registering the training images in the training stage. In order to save the computation time in the application stage, we predict only the initial deformations on the subject key points, which are detected automatically, as explained below.

Extraction of patch on each key point

To consistently and efficiently choose the key points from the subject image, rather than randomly selecting them, we follow the importance sampling strategy to hierarchically select the key points (Wang et al., 2010; Wu et al., 2012). Two criteria are used for selection of key points: (1) In a local view, key points should locate at the distinctive regions in the subject image, such as at sulcal root, gyral crown, and ventricular boundary, since points in these regions are relatively easy to identify for their correspondences; (2) In a global view, key points should cover the entire brain volume (i.e., the key points distributed in the whole brain) to derive the whole-brain deformation, while the density of key points should be high in the context-rich regions such as border of white matter and gray matter, while low in the context-uniform regions such as inside of the white matter. Specifically, we smooth and normalize the gradient magnitude values of intensities for all voxels in the subject image over the whole image domain. Then, we regard the obtained values as importance (or the probability) of each voxel to be selected as the key point. Higher importance value implies that the location under consideration is more likely to be drawn in non-uniform sampling, while lower value denotes lower chance for the respective location to be selected as a key point. Thus, based on this importance map, a set of key points can be sampled via Monte Carlo simulation. Fig. 2(a) shows the selected key points by the importance sampling as introduced above.

Suppose we have selected K key points X in the new testing subject image I_S. For each key point $x_k \in X$, we use $P_S(x_k)$ to denote the particular image patch in the new testing subject I_S, which is centered at the key point x_k. Similarly, we use $P_m(y)$ to denote a candidate image patch centered at the point $y \in n(x_k)$ of the training image I_m, where $n(x_k)$ denotes a search neighborhood centered at x_k. For each subject key point x_k under consideration, we can construct the over-complete coupled dictionary $D(x_k)$ by incorporating all possible candidate image patches $P_m(y)$ across all training images $\{I_m\}$, as well as the associated deformations $f_m(y)$ obtained in the training stage, i.e., $D(x_k) = \{(P_m(y), f_m(y)) | y \in n(x_k),\ m = 1, \ldots, N\}$.

It is worth noting that the size of each local subject patch $P_S(x_k)$ also needs to be adaptively determined since the scale of the local image content is highly related with the power in representing patch-based appearance. Intuitively, the patch size should be small at the areas with rich edge information (e.g., cortical area) in order to capture the complex local structural features, while the relatively large image patches should be used at the uniform regions (e.g., inside of the whiter matter) in order to make the image patch as distinctive as possible. Here, we adapt the Octree technique (Meagher, 1980) to efficiently

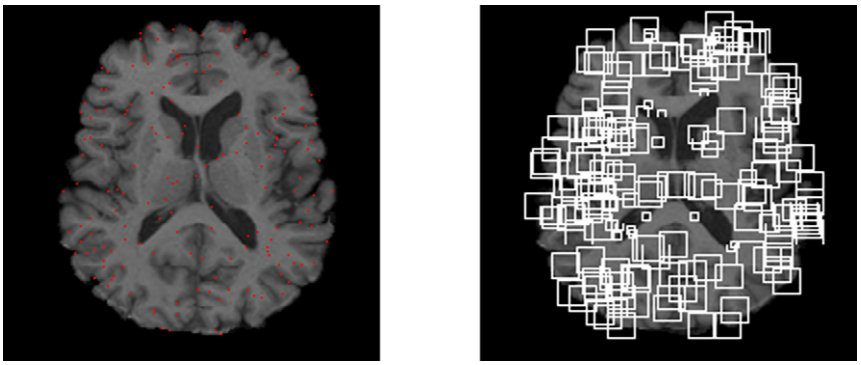

(a) Key points (b) Patches centered at the key points

Fig. 2. (a) The sampled key points and (b) the respective patches centered at the key points with adaptive sizes.

partition the whole brain into a set of blocks, where the size of each block is adaptive to the local image content. Specifically, the whole image is partitioned into 8 blocks equally in the beginning. Then, in each block, the intensity entropy is calculated. If the local entropy is higher than a certain threshold, further partitioning in the block is applied recursively until the intensity entropy drops below a certain threshold. Thus, for each subject key point x_k, we can finally acquire its associated block size (determined in the Octree-based partition) as the patch size. Fig. 2(b) displays the adaptively-determined patch sizes for the key points in Fig. 2(a).

Patch pre-selection

Patch pre-selection is applied here among all candidate patches when constructing the dictionary, in order to reduce the computational burden and also improve the prediction accuracy by excluding the irrelevant patches from the dictionary. Similar to the patch-based labeling approach (Coupé et al., 2011), the criterion γ for patch pre-selection is specially defined between $P_S(x_k)$ and $P_m(y)$ as follows:

$$\gamma(P_S(x_k), P_m(y)) = \frac{2\mu_S(x_k)\mu_m(y)}{[\mu_S(x_k)]^2 + [\mu_m(y)]^2} \times \frac{2\sigma_S(x_k)\sigma_m(y)}{[\sigma_S(x_k)]^2 + [\sigma_m(y)]^2} \quad (1)$$

where $\mu_S(x_k)$ and $\sigma_S(x_k)$ are the intensity mean and standard deviation in the local patch $P_S(x_k)$, respectively, and $\mu_m(y)$ and $\sigma_m(y)$ are the intensity mean and standard deviation in the local patch $P_m(y)$, respectively. Then, the new coupled local dictionary $D^*(x_k)$ at the subject key point x_k can be obtained as below:

$$D^*(x_k) = \{(P_m(y), f_m(y)) \mid y \in n(x_k),\ m = 1, \ldots, N,\ \gamma(P_S(x_k),\ P_m(y)) \rangle \Gamma\} \quad (2)$$

where Γ is the threshold used in patch pre-selection. Only if the value γ is greater than Γ, the patch $P_m(y)$ will be included in the dictionary; otherwise, this patch will be discarded. After this pre-selection procedure, we assume obtaining of Q elements in the dictionary $D^*(x_k)$ for the following sparse representation. For clarity, we use the column vector $\vec{\alpha}_q$ to denote the appearance of image patch $P_m(y)$ in $D^*(x_k)$, by using the bivariate index $q = (y, m)$. Similarly, we use the column vector $\vec{\beta}_q$ for the coupled deformation $f_m(y)$ in $D^*(x_k)$. The image patch $P_S(x_k)$ at the subject key point x_k is also vectorized as $\vec{\theta}$.

Deformation prediction by sparse patch representation

We here describe how to predict the local deformation on the subject key point x_k. The most straightforward way is to use non-local averaging of targets from all possible candidate patches in the coupled dictionary as described in Deformation prediction via non-local mean. On the other hand, we can also deploy the sparse representation to predict the local deformation by using only a small number of candidate patches (Deformation prediction by sparse representation). These two ways are described below one by one.

Deformation prediction via non-local mean

Originated from the non-local strategy which has been widely used in the computer vision area, such as image denoising and super-resolution (Buades et al., 2008; Protter et al., 2009; Manjón et al., 2010), most patch-based methods work in a non-local manner (Coupé et al., 2011). The overview of patch-based method is provided in Fig. 3. Specifically, all possible candidate patches from different training images are considered, with their contributions weighted by the patch similarities with respect to the subject patch, i.e.,

$$w_q = \exp\frac{-||\vec{\theta} - \vec{\alpha}_q||^2}{h^2}, \quad (3)$$

where w_q is the q-th element in the column weighting vector $\vec{w} = \left[w_q\right]_{q=1,\ldots,Q}$. The parameter h controls the strength of exponential penalty over the patch appearance similarity between the local patch $\vec{\theta}$ of each key point and the local training patch $\vec{\alpha}_q$. Then, for each point $x_k \in \Omega_{I_S}$ in the testing subject image I_S, the prediction of its initial deformation $f_S^E(x_k)$ can be estimated by using the weights estimated from the non-local mean as below:

$$f_S^E(x_k) = \frac{\sum_{q=1}^{Q} w_q \beta_q}{\sum_{q=1}^{Q} w_q}, \quad (4)$$

where β_q is the associated deformation to $\vec{\alpha}_q$.

Deformation prediction by sparse representation

While non-local mean is efficient, it has several limitations: (1) the discrimination power of excluding misleading patches can be limited

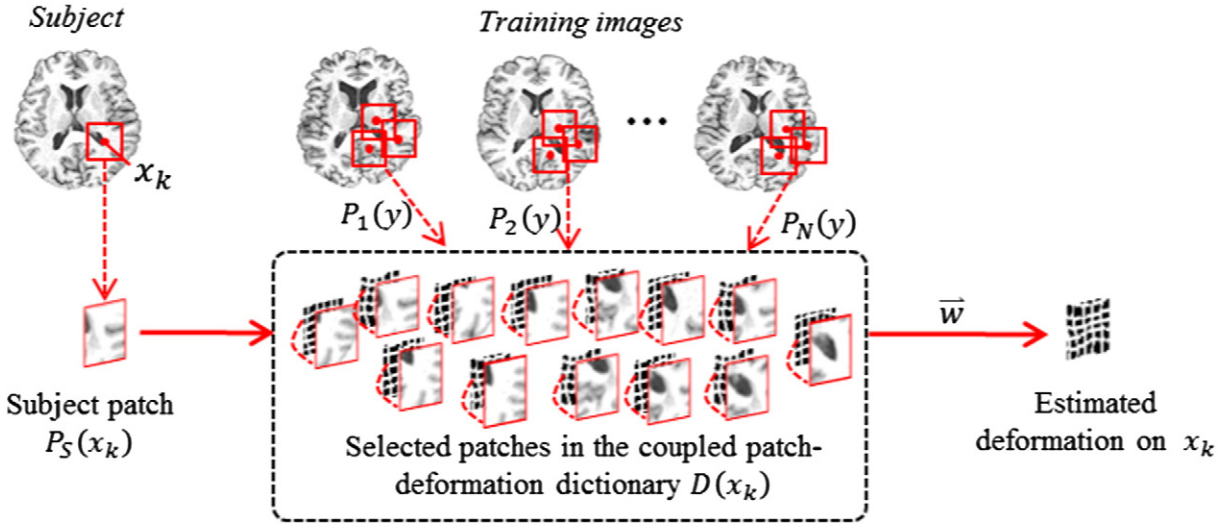

Fig. 3. The overview of the deformation estimation for one key point in a non-local manner. All candidate patches in the dictionary of training images contribute to the subject patch according to their individual weights in the vector $\vec{w}$, which is computed from patch similarities.

since all candidate patches in the training images, including some training patches apparently different from the subject patch in appearance, eventually contribute to the representation of the subject patch. Thus, the overall accuracy in predicting the deformation of the subject key point might be impacted negatively by these misleading training patches, although their individual weights might be low. (2) The non-local mean is very sensitive to the parameter h, which is usually determined in an empirical way for different applications.

To deal with the above issues, we use sparsity constraint for selecting only a small number of candidate training patches. Given the local dictionary $D^*(x_k)$ for each subject key point x_k, we seek for the sparse representation for its local appearance patch $\vec{\theta}$, which can be formulated in a well-known least absolute shrinkage and selection operator (LASSO) problem (Tibshirani, 1994). Specifically, we first assemble all Q local training patch appearances (represented by their respective column vectors) in the dictionary into a matrix $A = [\alpha_q]_{q=1,\ldots,Q}$. With the same order, we can also arrange their associated deformations $\{f_m(y)\}$ into a matrix $B = [\beta_q]_{q=1,\ldots,Q}$. Then, we can apply l_1-norm constraint on the weighting vector $\vec{w}$ to require that only a small number of similar patches in the dictionary should be selected to represent the subject patch $\vec{\theta}$. In this way, our method will become more robust to the outlier patches. Mathematically, the sparse coefficient vector $\vec{w}$ at each subject key point x_k can be estimated by solving the following optimization problem:

$$\hat{\vec{w}} = \text{argmin}_{\vec{w}} ||A\vec{w} - \vec{\theta}||^2 + \lambda ||\vec{w}||_1, \; s.t. \; w_q > 0, \tag{5}$$

where λ is a parameter controlling the strength of the l_1-norm regularization. This objective function can be optimized by Euclidian-projection based method as described in Liu and Ye (2009). After obtaining the sparse coefficient vector $\vec{w}$, the initial deformation on the subject key point x_k can be predicted by Eq. (4). The estimation of the sparse coefficient vector $\vec{w}$ and the prediction of the initial deformation $f_S^E(x_k)$ are demonstrated in Fig. 4.

Summary of our learning-based registration framework

Our registration method is capable of achieving robust registration results, with much less computation time, by predicting a good initial deformation field and then an intermediate template for a new subject image. The whole registration framework consists of two stages, i.e., training stage and the application stage, which are summarized below.

Training stage

Calculate N deformation fields $\{f_m | m = 1, \ldots, N\}$ by using an existing deformable registration method (e.g., HAMMER, diffeomorphic Demons, FNIRT, ART, or SyN) to register the template T with each of the N training images $\{I_m | m = 1, \ldots, N\}$.

Testing stage

1. Affine align the subject image I_S to the template I_T.
2. A set of K key points are first selected automatically in the subject image I_S.
3. Construct the coupled (appearance–deformation) local dictionary $D(x_k)$ for each subject key point x_k, by incorporating all possible can- didate image patches $\{P_m(y)\}$ from all training images as well as their associated deformations $\{f_m(y)\}$ at the center point y. Note that the patch size is adaptively determined by using the Octree technique.
4. Perform patch pre-selection and reduce the dictionary to contain Q coupled appearances and deformations.
5. Estimate the representation coefficient vector w by the sparse representation technique in Eq. 5.
6. Predict the initial deformation on the subject key point x_k by Eq. 4.
7. Perform Steps (3)–(6) for all key points in the subject image I_S.
8. Apply TPS interpolation to obtain the initial dense deformation field f_S^E by considering all subject key points as the source point set and their predicted local deformations as the target point set.
9. Deformthe template using the initial deformation field estimated in Step (8), and obtain the intermediate template.

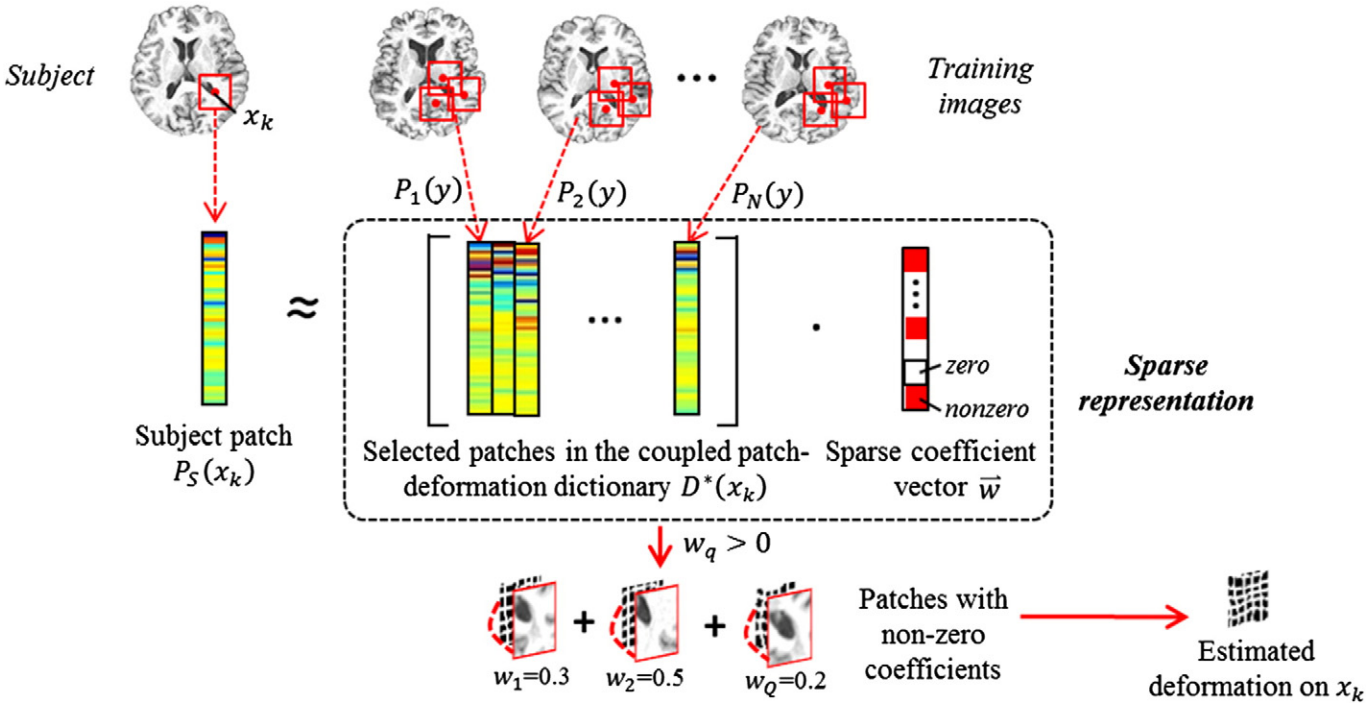

Fig. 4. Deformation prediction on a subject key point via sparse patch-based representation.

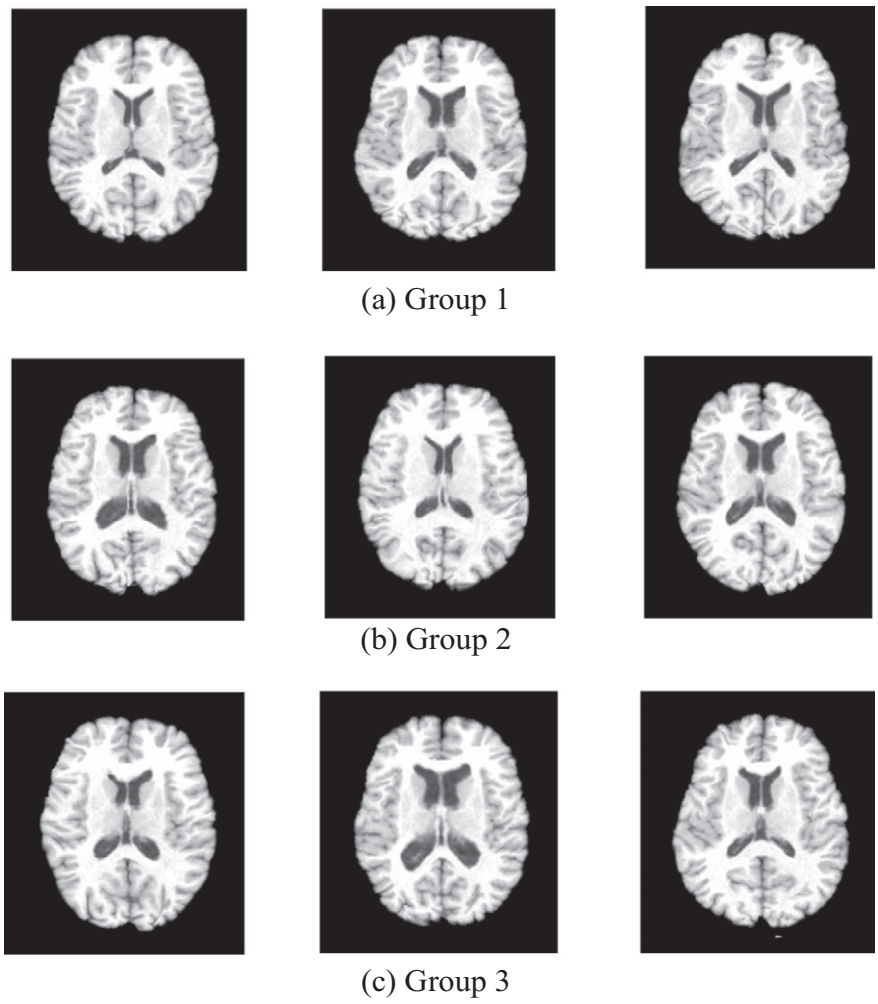

Fig. 5. Simulated images, generated by warping the template with the simulated deformation fields. According to the extent of deformations from the template, the simulated images can be classified into three groups: 3 mm (Group 1), 5 mm (Group 2), and 7 mm (Group 3).

10. Apply the existing deformable registration method to estimate the remaining deformation field between the intermediate template and the subject image.
11. Obtain the complete deformation field f_S by concatenating the initial dense deformation field f_S^E with the remaining deformation f_S^R estimated in Step (10).

Experimental results

We first used HAMMER, available in NITRC (http://www.nitrc.org/projects/hammer_suite), as a baseline method to demonstrate the benefit of patch-based deformation prediction for image registration. Moreover, to examine the advantage of sparse patch representation, we compared our method with a degenerated version, i.e., non-local mean. The results were also compared with our previous global regression-model-based deformation prediction method (Kim et al., 2012). The elderly brain images demonstrated in Experiments on elderly brains were used to determine the values for all parameters, i.e., the criterion γ for patch pre-selection in Eq. (1), the decay parameter h in Eq. (3), and the strength λ of the l_1-norm regularization in Eq. (5). Specifically, we followed the parameter setting in a non-local means study (Coupé et al., 2011) to set $\gamma = 0.98$ and allow h to be adapted to the minimum distance of all candidate patches. We also fixed $\lambda = 0.4$ for all image datasets.

It is worth noting that our proposed sparse patch-based method owns the general capability to improve the registration performance of many existing deformable registration methods. To this end, we also tested other widely-used deformable registration algorithms, e.g., FNIRT (Andersson et al., 2008), SyN (Avants et al., 2008), ART (Ardekani et al.,

Table 1
Mean deformation prediction error, compared to the simulated ground-truth deformations in mm. The asterisks denote the statistical significance on the deformation prediction errors by different methods via two-sample *t*-tests w.r.t. the sparse patch-based method (***: $p < 0.01$, **: $p < 0.05$ and *: $p < 0.1$).

	Group 1	Group 2	Group 3	Average
Regression-model-based	1.88**	2.26**	2.72***	2.29
Non-local patch-based	1.69*	2.02**	2.31**	2.01
Sparse patch-based	1.54	1.81	1.96	1.77

Table 2
Mean registration error, compared to the simulated ground-truth deformations in mm. The asterisks denote the statistical significance on the registration errors by different methods via two-sample *t*-tests w.r.t. HAMMER + Sparse method (***: $p < 0.01$, **: $p < 0.05$ and *: $p < 0.1$).

	Group 1	Group 2	Group 3	Average
HAMMER	0.45**	0.53***	0.64***	0.54
HAMMER + Regression	0.38**	0.42**	0.51**	0.44
HAMMER + Non-local	0.36*	0.39*	0.48**	0.41
HAMMER + Sparse	0.34	0.36	0.43	0.38

2005), and diffeomorphic Demons (Vercauteren et al., 2009), after integrated with our patch-guided deformation prediction framework. Regardless of different registration algorithms incorporated in our framework, all above-mentioned parameters γ, h, and λ were kept same.

Experiments on simulated data

We used the algorithm proposed in Xue et al. (2006) to generate 30 simulated brain images, thus the simulated deformation fields are considered as the ground-truth for evaluation. The mean magnitude of the ground-truth deformation fields was set to 5 mm during simulation. As displayed in Fig. 5, the simulated images are grouped into 3 groups according to their perturbed deformation amounts. Group 1 includes the images with the relatively small deformations, while Group 3 includes the images with large deformations. For example, the average magnitude of deformations in Group 1 is 3 mm, while the average magnitudes of deformations in Groups 2 and 3 are 5 mm and 7 mm, respectively. Then, we applied two patch-based prediction methods, i.e., the non-local mean patch-based method and the sparse patch-based method, to predict the initial deformation field for each simulated image, by using the rest images as training images. We further compared the performance of the patch-based prediction methods with a deformation prediction method using a global statistical model, i.e., the regression-model-based deformation prediction method in Kim et al. (2012). Table 1 compares the mean of the deformation prediction errors obtained by three deformation prediction methods. As we can see, our sparse patch-based method achieves the lowest residual error, with respect to the simulated ground-truth deformation fields, thus showing the best deformation prediction performance among the three prediction methods. Furthermore, greater improvement can be observed in Group 3 (with larger magnitudes of the simulated deformations) than in other two groups. Also, our proposed method consistently works better than other two methods even for the images with large deformations. In Table 1, we specifically added the p-values by performing two-sample t-tests on deformation prediction errors by our sparse patch-based method compared with those by other two methods (e.g., regression-model-based and non-local patch-based methods) in Groups 1–3. As shown in Table 1, the p-values are mostly smaller than 0.05, thus indicating the statistical significance of the difference in deformation prediction errors between sparse patch-based method and other two methods. On the other hand, we observed that all p-values from two-sample t-tests on the deformation prediction errors between regression-model-based and non-local patch-based methods were smaller than 0.05, regardless of different groups, thus also showing the statistical significance.

The residual deformation could be further estimated by applying an existing deformable registration algorithm, such as HAMMER. Table 2 compares the mean registration error obtained by four different registration methods, i.e., HAMMER without deformation prediction, HAMMER + Regression (Kim et al., 2012), HAMMER + Non-Local, and HAMMER + Sparse, for those three image groups. Note that we use the same registration parameters for all these four methods. As shown in Table 2, our HAMMER + Sparse method achieves the lowest residual error w.r.t. the simulated ground-truth deformation fields, and also more registration improvement in Group 3 than other two groups. This also indicates that our prediction method can provide better initialization than other prediction methods. Similar to the statistical significance tests on deformation prediction performance as demonstrated in Table 1, the two-sample t-tests on the registration errors by our HAMMER + Sparse and three other methods (HAMMER, HAMMER + Regression, and HAMMER + Non-Local) were also performed and provided in Table 2. Specifically, for Group 3, HAMMER + Sparse shows the statistical significance over all other methods in terms of registration error. We also performed, respectively, the two-sample t-tests among HAMMER, HAMMER + Regression and HAMMER + Non-Local, and found that all p-values are smaller than 0.05. Specifically, the difference of registration error of HAMMER + Regression compared to HAMMER is statistically better (with most p-values smaller than 0.01). This indicates that all methods with initialization (e.g., HAMMER + Regression, HAMMER + Non-Local, and HAMMER + Sparse) outperform HAMMER alone, while patch-based methods (e.g., HAMMER + Non-Local and HAMMER + Sparse) are still better than HAMMER + Regression, and HAMMER + Sparse shows the best performance.

To inspect the deformation prediction performance in the local brain regions, we further measured the averaged voxel-wise deformation discrepancies on 93 ROIs separately, between the estimated deformations by the four registration methods and the simulated ground-truth deformations. Compared to the original HAMMER algorithm without deformation initialization, our proposed prediction method + HAMMER (i.e., HAMMER + Sparse) achieved comparable performance on 39 ROIs, while the significantly lower deformation errors on 54 ROIs with paired t-test. The maximum reduction of the deformation error is 2.62 mm. The other two registration schemes with initial deformation predictions, i.e., HAMMER + Regression and HAMMER + Non-Local, have the significantly lower deformation errors only on 22 and 38 ROIs, compared to the baseline HAMMER registration method, respectively. Specifically, the maximum reductions of deformation errors are 1.54 mm for HAMMER + Regression and 2.03 mm for HAMMER + Non-Local. Again, these results indicate that our method can improve the final registration accuracy by predicting more accurate initial deformation field.

Experiments on elderly brains

In this experiment, we evaluated not only the accuracy of the predicted initial deformation fields but also the benefit of using local adaptive patch size in the sparse representation of patches (Extraction of patch on each key point).

Quantitative measure of intermediate template

In the training stage, we estimated the deformation fields for 50 images with respect to the template (Fig. 6(a)) by HAMMER. These 50 training images and the template were randomly selected from a MR brain image database consisting of elderly brains aged from 65 to 80. To evaluate the quality of the initial deformations estimated by the three prediction methods, i.e., the regression-model-based method (Kim et al., 2012), non-local patch-based method, and the sparse patch-based method, we applied these three methods to predict the initial deformations on 30 new subject images (which are not used for training) in the application stage. Accordingly, we can obtain 30 intermediate templates, corresponding to the 30 subject images, by each prediction method. For quantitative evaluation of those estimated intermediate templates, we calculated the Dice ratios (VanRijsbergen, 1979) for those 30 subjects, to measure the overlaps of white matter (WM), gray matter (GM), and ventricular cerebrospinal fluid (VN) between each pair of subject image and its respective intermediate template. The Dice ratios by three methods are shown in Table 3. It is apparent that our proposed sparse patch-based deformation prediction method achieves higher Dice ratios than both regression-based and non-local patch-based deformation prediction methods for all three tissue types. In Table 3, we specifically added the p-values by performing two-sample t-tests on the overlap ratios of WM, GM and VN by our sparse patch-based method compared with those by other two methods (e.g., regression-model-based and non-local patch-based methods). As shown in Table 3, all p-values are smaller than 0.05, indicating statistical difference between our sparse patch-based method and other two methods. On the other hand, all p-values from two-sample t-tests on the overlap ratios of WM, GM and VN between regression-model-based and non-local patch-based methods were also found to be smaller than 0.05, thus also showing the statistical significance of these methods.

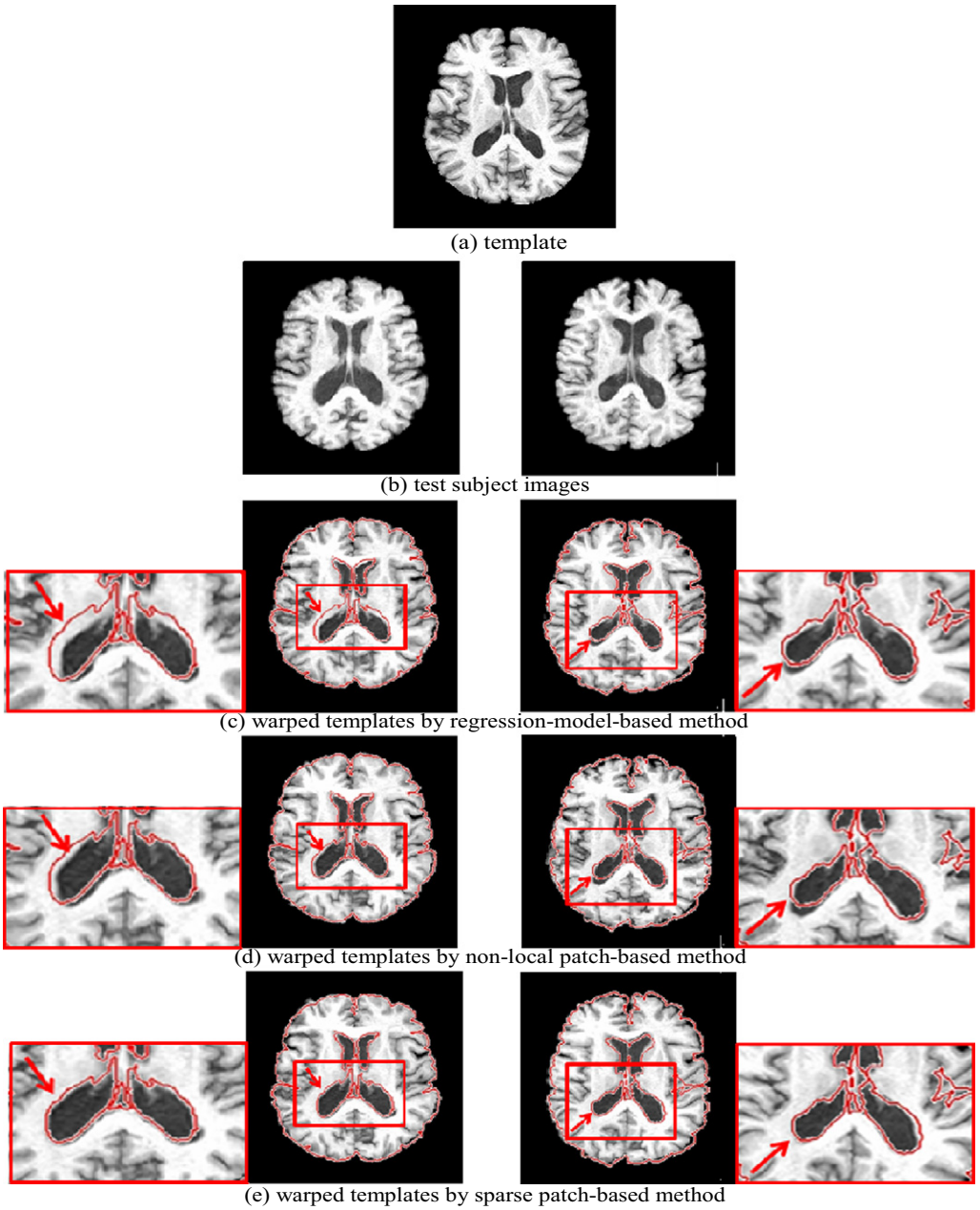

Fig. 6. Demonstration of generating intermediate templates for two typical subject images in (b), by predicting the initial deformations with the regression-model-based method (c), non-local patch-based method (d), and our proposed sparse patch-based method (e), respectively. Compared to the subject images in (b), the resulting intermediate templates by our proposed method are more similar (i.e., as pointed by the red arrows in the enlarged views) than those by the other two prediction methods. For visual comparison, the outlines of the whole brain volumes and ventricles are also extracted from the subject images and overlaid onto the respective intermediate templates.

To examine the effect of using adaptive patch size, we computed the average overlap ratios of WM, GM, and VN calculated from 30 subjects (described above) by the sparse patch-based method with different pre-determined patch sizes. Note that, in our proposed method, the patch size is adaptively determined by the Octree-based partition, which can vary from $3 \times 3 \times 3$ mm^3 to $11 \times 11 \times 11$ mm^3. We examined the Dice ratio between the subject image and the intermediate template

Table 3
Average overlap ratios of WM, GM and VN, computed based on 30 subjects after deformation prediction with the regression-model-based, non-local patch-based, and sparse patch-based methods, respectively. The asterisks denote the statistical significance on the overlap ratios by different methods via two-sample *t*-tests w.r.t. the sparse patch-based method (***: $p < 0.01$, **: $p < 0.05$ and *: $p < 0.1$).

	WM	GM	VN	Overall
Regression-model-based	75.5%***	68.9%**	82.2%***	75.5%
Non-local patch-based	77.0%**	69.8%**	84.5%**	77.1%
Sparse patch-based	78.5%	71.4%	87.3%	79.1%

Table 4
Average overlap ratios (%) of WM, GM and VN, computed based on 30 testing subjects after deformation prediction by *the sparse patch-based methods with different settings of patch size*. The asterisks denote the statistical significance on the overlap ratios by our method with fixed patch sizes w.r.t. our method with adaptive patch size (***: $p < 0.01$, **: $p < 0.05$ and *: $p < 0.1$).

	WM	GM	VN	Overall
Fixed patch size ($3 \times 3 \times 3$)	77.4%**	70.4%**	85.3%**	77.7%
Fixed patch size ($7 \times 7 \times 7$)	77.4%**	70.2%**	85.1%**	77.6%
Fixed patch size ($11 \times 11 \times 11$)	77.2%**	70.1%**	84.9%***	77.4%
Adaptive patch size	78.5%	71.4%	87.3%	79.1%

based on the initial deformation fields predicted by using the adaptive patch sizes or by using the fixed patch sizes, respectively. The results shown in Table 4 indicate that the adaptive determination of patch size can significantly help predict more accurate initial deformation fields than using the fixed patch size. Also, the two-sample *t*-tests between all overlap ratios by *our sparse patch-based method with adaptive patch size* and those by *other three cases with fixed patch sizes* indicated the statistically significant differences of overlap ratios (with all *p*-values smaller than 0.05).

Visual inspection of intermediate template

We hereby compared the closeness between the generated intermediate template and the test subject in each deformation prediction method. Through visual inspection in Fig. 6, we can see that our method (Fig. 6(e)) is able to estimate the initial deformation for bringing the template closer to the respective test subject image, compared to the regression-model-based method (Fig. 6(c)) and also the non-local patch-based method (Fig. 6(d)). To help visual comparison, we delineated the outline of the brain volume and also the contour of the ventricle of each test subject image (as shown with the red curves), and superimposed the drawings on the intermediate templates generated by different deformation prediction methods. It can be observed that the intermediate templates generated by the patch-based deformation prediction methods are generally better than those by the regression-model-based method. Closer inspection further shows that the intermediate templates generated by the sparse patch-based deformation prediction method are much closer (in terms of structure shapes) to the test subject images than those by the other two methods, especially in the regions highlighted by the red arrows.

Registration performance

The remaining deformation from each intermediate template to each test subject image can be further estimated by HAMMER. For quantitative evaluation of registration performance by incorporating each of three deformation prediction methods, we calculated the Dice ratios for those 30 subjects mentioned in Quantitative measure of intermediate template, to measure the overlaps of WM, GM, and VN between the finally registered subject images and the template. The Dice ratios by three methods, as well as the result by HAMMER, are shown in Table 5. The comparison results indicate that HAMMER with incorporation of each of three deformation prediction methods outperforms HAMMER without deformation initialization. It is also apparent that our proposed sparse patch-based deformation prediction method achieves higher Dice ratios than both regression-based and non-local patch-based deformation prediction methods, for all three tissue types. The two-sample *t*-tests on the overlap ratios of WM, GM and VN by our HAMMER + Sparse and three other methods (HAMMER, HAMMER + Regression, and HAMMER + Non-Local) are shown in Table 5. Specifically, for GM and VN, HAMMER + Sparse shows statistical significance over all other methods, in terms of overlap ratio. We also performed, respectively, the two-sample *t*-tests among HAMMER, HAMMER + Regression and HAMMER + Non-Local, and found that all *p*-values were smaller than 0.05. In particular, the difference in overlap ratio of HAMMER + Regression compared to HAMMER was statistically better (with most *p*-values smaller than 0.01). This indicates that all methods with initialization (e.g., HAMMER + Regression, HAMMER + Non-Local, and HAMMER + Sparse) outperform HAMMER alone, while patch-based methods (e.g., HAMMER + Non-Local and HAMMER + Sparse) are still better than HAMMER + Regression, and HAMMER + Sparse shows the best performance.

Table 5
Average overlap ratios of WM, GM and VN, computed based on the 30 testing subjects aligned, respectively, by HAMMER, HAMMER + Regression, HAMMER + Non-local and HAMMER + Sparse methods to a template. The asterisks denote the statistical significance on the overlap ratios by different methods via two-sample *t*-tests w.r.t. HAMMER + Sparse method (***: $p < 0.01$, **: $p < 0.05$ and *: $p < 0.1$).

	WM	GM	VN	Overall
HAMMER	82.3%**	72.0%***	88.5%***	80.9%
HAMMER + Regression	83.2%**	73.1%**	89.3%**	81.9%
HAMMER + Non-local	83.7%*	74.0%**	89.7%**	82.5%
HAMMER + Sparse	84.0%	74.3%	90.2%	82.8%

Performance of deformation prediction and registration on LONI LPBA40 dataset

The LONI LPBA40 dataset (Shattuck et al., 2008) consists of 40 images, each with 54 manually-labeled ROIs. After selecting one individual image as the template, we used the remaining 20 images for training and other 19 images as test subject images. To evaluate the prediction accuracy, the template image was first warped toward the 19 subjects by applying the initial deformations predicted by the regression-model-based method, non-local patch-based method, and our proposed sparse patch-based method. Then, the Dice ratios for all ROIs between each subject image and its corresponding intermediate template image, yielded by those three methods, were computed for quantitative comparison. The obtained average Dice ratios over all 19 subjects were 54.7% by the regression-model-based method, 56.7% by the non-local patch-based method, and 58.6% by our sparse patch-based method. According to the two-sample *t*-tests on the average Dice ratios over 19 subjects for all 54 ROIs performed between our HAMMER + Sparse and two other methods (i.e., HAMMER and HAMMER + Regression), the improvement by HAMMER + Sparse was statistically significant ($p < 0.01$). HAMMER + Regression also showed the statistical significance (with p-value < 0.05) compared with HAMMER, in terms of overlap ratios on 54 ROIs. Specifically, our sparse patch-based method achieved higher overlap scores on 38 out of 54 ROIs (with the maximum improvement of 8.1%) than the regression-model-based method, while the non-local patch-based method achieved higher overlap scores in 29 out of 54 ROIs (with the maximum improvement of 5.9%) than the regression-model-based method.

The remaining deformation from each intermediate template to each test subject image can be further estimated by HAMMER. Compared with the direct registration of template to subject by HAMMER, our HAMMER + Sparse method obtained higher average Dice overlap ratio (72.5%) than HAMMER (71.0%) and HAMMER + Regression (71.8%). In Fig. 7, we show the Dice overlap ratio of each ROI for HAMMER (in blue), HAMMER + Regression (in green), and HAMMER + Sparse method (in pink), indicating that our integrated framework yields better registration performance (in terms of higher tissue overlap ratios) for most ROIs than HAMMER without deformation initialization.

It is worth noting that our framework is general enough to allow for the incorporation of other registration algorithms. Thus, besides HAMMER, we also integrate our sparse patch-based deformation prediction method with diffeomorphic Demons, FNIRT, ART, and SyN registration algorithms. That is, for each registration method, we use it to register the training images in the training stage, which provides the training deformations to construct the coupled dictionary. To register with the new test subject image, we apply our sparse patch-based prediction method to predict the initial deformation field. Finally, we use the respective registration method again to estimate the remaining deformation between the intermediate template and the subject, as shown in Fig. 1. Note that our intention here is not to compare the performances of the individual registration methods, e.g., HAMMER, diffeomorphic Demons, FNIRT, ART and SyN, but to demonstrate the improvement after integrating our sparse patch-based deformation prediction framework into these methods.

Since the software of ART and SyN does not provide the interfaces to use the initial deformation field, the integrated versions of these two methods consider the intermediate template images as the target image in their standard registration procedure. That is, for each new

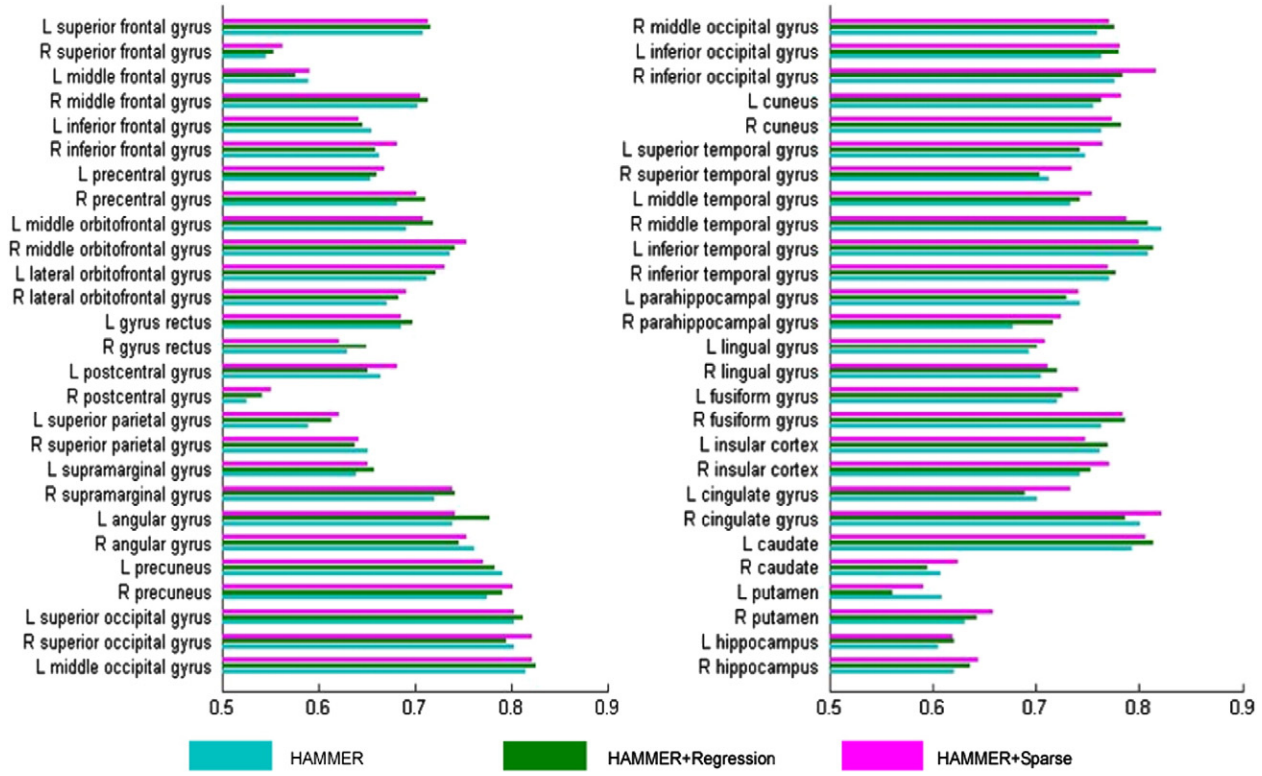

Fig. 7. Average overlap ratios of the 54 aligned ROIs by HAMMER, HAMMER + Regression, and HAMMER + Sparse, respectively. Two-sample *t*-tests between HAMMER + Sparse and other two methods (HAMMER and HAMMER + Regression) show the statistical significance ($p < 0.01$).

testing subject image, we first use our method to estimate the intermediate template and then use ART (or SyN) to estimate the deformation between the subject and the intermediate template. By using the same dataset (i.e., 1 image in LONI LPBA40 dataset as the template, 20 images for training, and the rest 19 images as the test subject images), the average Dice ratio of the 19 test subject images by 5 registration methods, before and after integrating our sparse patch-based deformation prediction framework, is listed in Table 6. The five sets of two-sample *t*-tests on the average Dice ratios over 19 test subjects for all 54 ROIs by five pairs of registration methods *before and after integrating our sparse patch-based deformation prediction framework* showed statistical significance in improvement of the average Dice ratio (with all *p*-values smaller than 0.05) as shown in Table 6.

Computation time

Since our method can predict the initial deformation field, the registration time can also be reduced significantly by applying only the existing registration methods to estimate the small remaining deformation field. By taking LONI LPBA40 dataset (with a size of $220 \times 220 \times 184$ for each image) for example, we compared the average computation time costs of the direct registration and the indirect registration with the use of our predicted initial deformation field. The computation time before and after using our estimated initial deformation field by HAMMER, diffeomorphic demons, FNIRT, ART and SyN are shown in Table 7. It is clear that the reduction of computation time can be up to 4–7 folds for all five registration methods after integrating our predictions.

Note that, in predicting the initial deformation field by sparse representation, we used parallel programming on 16 CPUs to speed up the prediction time. In our experiment, the non-local patch-based method and the sparse patch-based method take 8 minutes and 4 min, respectively, for deformation prediction.

Discussion and conclusion

A novel patch-based deformation prediction framework has been proposed in this paper for improving the registration performance of the existing registration algorithms. Specifically, we assume that, if two image patches have similar appearance, they should follow similar deformations toward the same template image. Thus, we construct a coupled local adaptive dictionary, for each subject key point, with the patch-based image appearances and deformations obtained from the training images. By using the sparse representation technique to find the sparse coefficients for the subject image patch appearance with patch appearances in the constructed dictionary, we can predict the

Table 6
Average Dice ratio by HAMMER, diffeomorphic Demons, FNIRT, ART and SyN, before and after integrating our sparse patch-based deformation prediction framework. The asterisks denote the statistical significance on the overlap ratios over 19 subjects by different registration algorithms *before integrating our sparse patch-based deformation prediction framework* w.r.t. those *after integrating our sparse patch-based deformation prediction framework* (***: $p < 0.01$, **: $p < 0.05$ and *: $p < 0.1$).

	HAMMER	Diff. Demons	FNIRT	ART	SyN
Before	71.0%***	70.3%***	69.7%**	70.5%**	72.4%***
After	72.5%	72.2%	71.0%	71.6%	73.5%

Table 7
Comparison of computation times for HAMMER, diffeomorphic Demons, FNIRT, ART and SyN before and after integrating our sparse patch-based deformation prediction framework (unit: minute).

	HAMMER	Diff. Demons	FNIRT	ART	SyN
Before	28	4	40	12	31
After	5	1	11	3	8

initial deformation for each subject key point by applying the same sparse coefficients onto the coupled deformation dictionary.

Since our sparse patch-based prediction method is fully adaptive to the local image content, our proposed method is flexible to improve the registration performance of the conventional registration methods than other global learning-based methods (Kim et al., 2012), which consider the entire image as a whole for prediction. It is worth noting that, to make the computation efficient, we only use the simple intensity information for sparse patch representation. In the future, we will test using more image features to make the sparse patch representation and deformation prediction more robust. Our future work also includes incorporation of our proposed prediction method with more existing registration algorithms (Shen et al. 1999, Zacharaki et al. 2008, Yang et al. 2008, Zacharaki et al. 2009, Wu et al. 2011, Wu et al. 2012), such as the B-Spline based registration method (Rueckert et al., 1999), and then tests their performances on more image datasets (beyond the brain images).

Acknowledgment

This work was supported in part by NIH grants EB006733, EB008374, EB009634, MH100217, AG042599 and AG041721. This work was also supported by ICT R&D program of MSIP/IITP (14-824-09-014, Basic Software Research in Human-level Lifelong Machine Learning) funded by the Korean government.

References

Albrecht, T., Luthi, M., et al., 2008. A Statistical Deformation Prior for Non-rigid Image and Shape Registration. Computer Vision and Pattern Recognition, 2008. CVPR 2008. IEEE Conference on.
Andersson, J., Smith, S., et al., 2008. FNIRT — FMRIB's Non-linear Image Registration Tool. Fourteenth Annual Meeting of the Organization for Human Brain Mapping — HBM.
Ardekani, B.A., Guckemus, S., et al., 2005. Quantitative comparison of algorithms for inter-subject registration of 3D volumetric brain MRI scans. J. Neurosci. Methods 142 (1), 67–76.
Avants, B.B., Epstein, C.L., et al., 2008. Symmetric diffeomorphic image registration with cross-correlation: evaluating automated labeling of elderly and neurodegenerative brain. Med. Image Anal. 12 (1), 26–41.
Bajcsy, R., Kovacic, S., 1989. Multiresolution elastic matching. Comput. Vis. Graph. Image Process. 46.
Bookstein, F.L., 1989. Principal warps: thin-plate splines and the decomposition of deformations. IEEE Trans. Pattern Anal. Mach. Intell. 11 (6), 567–585.
Buades, A., Coll, B., et al., 2008. Nonlocal image and movie denoising. Int. J. Comput. Vis. 76 (2), 123–139.
Chatterjee, P., Milanfar, P., 2012. Patch-based near-optimal image denoising. IEEE Trans. Image Process. 21 (4), 1635–1649.
Chen, Y., An, H., et al., 2009. White matter abnormalities revealed by diffusion tensor imaging in non-demented and demented HIV+ patients. Neuroimage 47 (4), 1154–1162.
Christensen, G., Rabbitt, R.D., et al., 1994. 3D brain mapping using a deformable neuroanatomy. Phys. Med. Biol. 39, 609–618.
Christensen, G., Rabbitt, R.D., et al., 1996. Deformable templates using large deformation kinematics. IEEE Trans. Med. Imaging 5 (10), 1435–1447.
Coupé, P., Manjón, J.V., et al., 2011. Patch-based segmentation using expert priors: application to hippocampus and ventricle segmentation. NeuroImage 54 (2), 940–954.
Davatzikos, C., 1997. Spatial transformation and registration of brain images using elastically deformable models. Comput. Vis. Image Underst. 66 (2), 207–222.
Downhill, J.E., Buchsbaum, M.S., et al., 2000. Shape and size of the corpus callosum in schizophrenia and schizotypal personality disorder. Schizophr. Res. 42 (3), 193–208.
Ferrant, M., Warfield, S., et al., 2000. Registration of 3D Intraoperative MR Images of the Brain Using a Finite Element Biomechanical Model. Third International Conference on Medical Image Computing and Computer-assisted Intervention, Pittsburgh, PA.
Freeborough, P.A., Fox, N.C., 1998. Modeling brain deformations in Alzheimer's disease by fluid registration of serial 3D MR images. J. Comput. Assist. Tomogr. 22, 838–843.
Frisoni, G., Testa, C., et al., 2002. Detection of grey matter loss in mild Alzheimer's disease with voxel based morphometry. J. Neurol. Neurosurg. Psychiatry 73, 657–664.
Glocker, B., Komodakis, K., et al., 2009. Dense registration with deformation priors. IPMI LNCS 5636, 540–551.
Job, D.E., Whalley, H.C., et al., 2003. Voxel-based morphometry of grey matter densities in subjects at high risk of schizophrenia. Schizophr. Res. 64 (1), 1–13.
Johnson, H.J., Christensen, G.E., 2002. Consistent landmark and intensity-based image registration. IEEE Trans. Med. Imaging 21 (5), 450–461.
Kim, M., Wu, G., et al., 2012. A general fast registration framework by learning deformation–appearance correlation. IEEE Trans. Image Process. 21 (4), 1823–1833.
Liu, J., Ye, J., 2009. Efficient Euclidean Projections in Linear Time. Proceedings of the 26th Annual International Conference on Machine Learning Montreal, Quebec, Canada. ACM, pp. 657–664.
Loeckx, D., Makes, F., et al., 2003. Non-rigid image registration using a statistical spline deformation model. IPMI LNCS 2732, 463–474.
Manjón, J.V., Coupé, P., et al., 2010. Adaptive non-local means denoising of MR images with spatially varying noise levels. J. Magn. Reson. Imaging 31 (1), 192–203.
Meagher, D., 1980. Octree Encoding: A New Technique for the Representation, Manipulation and Display of Arbitrary 3-D Objects by Computer. Technical, Report IPL-TR-80–111. ensselaer Polytechnic Institute.
Merschhemke, M., Mitchell, T.N., et al., 2003. Quantitative MRI detects abnormalities in relatives of patients with epilepsy and malformations of cortical development. NeuroImage 18 (3), 642–649.
Neu, S., Toga, A., 2008. Automatic localization of anatomical point landmarks for brain image processing algorithms. Neuroinformatics 6 (2), 135–148.
Ou, Y., Sotiras, A., et al., 2011. DRAMMS: deformable registration via attribute matching and mutual-saliency weighting. Med. Image Anal. 15 (4), 622–639.
Protter, M., Elad, M., et al., 2009. Generalizing the nonlocal-means to super-resolution reconstruction. IEEE Trans. Image Process. 18 (1), 36–51.
Qiao, H., Zhang, H., et al., 2009. Embryonic stem cell grafting in normal and infarcted myocardium: serial assessment with MR imaging and PET dual detection. Radiology 250 (3), 821–829.
Rohr, K., 1999. Image Registration Based on Thin-plate Splines and Local Estimates of Anisotropic Landmark Localization Uncertainties. MICCAI.
Rousseau, F., Habas, P.A., et al., 2011. A supervised patch-based approach for human brain labeling. IEEE Trans. Med. Imaging 30 (10), 1852–1862.
Rueckert, D., Sonoda, L.I., et al., 1999. Non-rigid registration using free-form deformations: application to breast MR images. IEEE Trans. Med. Imaging 18 (8), 712–721.
Rueckert, D., Frangi, A., et al., 2003. Automatic construction of 3-D statistical deformation models of the brain using nonrigid registration. IEEE Trans. Med. Imaging 22 (8), 1014–1025.
Shattuck, D.W., Mirza, M., et al., 2008. Construction of a 3D probabilistic atlas of human cortical structures. NeuroImage 39 (3), 1064–1080.
Shen, D., 2004. Image Registration by Hierarchical Matching of Local Spatial Intensity Histograms. MICCAI, St. Malo, France (Springer-Verlag GmbH).
Shen, D., Davatzikos, C., 2002. HAMMER: hierarchical attribute matching mechanism for elastic registration. IEEE Trans. Med. Imaging 21 (11), 1421–1439.
Shen, D., Davatzikos, C., 2003. Very high resolution morphometry using mass-preserving deformations and HAMMER elastic registration. NeuroImage 18 (1), 28–41.
Shen, D., Lao, Z., et al., 2004. Optimized prostate biopsy via a statistical atlas of cancer spatial distribution. Med. Image Anal. 8 (2), 139–150.
Smola, A.J., Scholköpf, B., 2004. A tutorial on support vector regression. Stat. Comput. 14, 199–222.
Shen, D., Wong, W.h., et al., 1999. Affine-invariant image retrieval by correspondence matching of shapes. Image Vis. Comput. 17 (7), 489–499.
Tang, S., Fan, Y., et al., 2009. RABBIT: rapid alignment of brains by building intermediate templates. Neuroimage 47 (4), 1277–1287.
Thirion, J.P., 1998. Image matching as a diffusion process: an analogy with Maxwell's demons. Med. Image Anal. 2 (3), 243–260.
Thompson, P.M., Mega, M.S., et al., 2001. Cortical change in Alzheimer's disease detected with a disease-specific population-based brain atlas. Cereb. Cortex 11 (1), 1–16.
Tibshirani, R., 1994. Regression shrinkage and selection via the lasso. J. R. Stat. Soc. 58, 267–288.
VanRijsbergen, C.J., 1979. Information Retrieval. Butterworth-Heinemann, London.
Vercauteren, T., Pennec, X., et al., 2009. Diffeomorphic demons: efficient non-parametric image registration. Neuroimage 45 (Supplement 1), S61–S72.
Verma, R., Mori, S., et al., 2005. Spatiotemporal maturation patterns of murine brain quantified by diffusion tensor MRI and deformation-based morphometry. Proc. Natl. Acad. Sci. U. S. A. 102 (19), 6978–6983.
Wang, Q., Wu, G., et al., 2010. Attribute vector guided groupwise registration. Neuroimage 50 (4), 1485–1496.
Wu, G., Jia, H., et al., 2011. SharpMean: groupwise registration guided by sharp mean image and tree-based registration. Neuroimage 56 (4), 1968–1981.
Wu, G., Kim, M., et al., 2014. S-HAMMER: hierarchical attribute-guided, symmetric diffeomorphic registration for MR brain images. Hum. Brain Mapp. 35 (3), 1044–1060.
Wu, G., Wang, Q., et al., 2012. Feature-based groupwise registration by hierarchical anatomical correspondence detection. Hum. Brain Mapp. 33 (2), 253–271.
Xue, Z., Shen, D., et al., 2006. Statistical representation of high-dimensional deformation fields with application to statistically-constrained 3D warping. Med. Image Anal. 10 (5), 740–751.
Yang, J., Shen, D., et al., 2008. Diffusion tensor image registration using tensor geometry and orientation features. Medical Image Computing and Computer-Assisted Intervention 5242, 905–913.
Zacharaki, E.I., Dinggang, S., et al., 2008. ORBIT: a multiresolution framework for deformable registration of brain tumor images. Medical Imaging. IEEE Trans. on 27 (8), 1003–1017.
Zacharaki, E.I., Hogea, C.S., et al., 2009. Non-diffeomorphic registration of brain tumor images by simulating tissue loss and tumor growth. Neuroimage 46 (3), 762–774.
Zhang, Y., Wu, G., et al., 2012. Hierarchical patch-based sparse representation: a new approach for resolution enhancement of 4D-CT lung data. IEEE Trans. Med. Imaging 31 (11), 1993–2005.
Zhou, S., Comaniciu, D., 2007. Shape regression machine. IPMI (Information Processing in Medical Imaging). LNCS 4584, 13–25.
Zongben, X., Jian, S., 2010. Image inpainting by patch propagation using patch sparsity. IEEE Trans. Image Process. 19 (5), 1153–1165.